

Tune-out and magic wavelengths for ground-state $^{23}\text{Na}^{40}\text{K}$ molecules

Roman Bause,^{1,2,*} Ming Li,³ Andreas Schindewolf,^{1,2} Xing-Yan Chen,^{1,2}
 Marcel Duda,^{1,2} Svetlana Kotochigova,³ Immanuel Bloch,^{1,2,4} and Xin-Yu Luo^{1,2}

¹*Max-Planck-Institut für Quantenoptik, 85748 Garching, Germany*

²*Munich Center for Quantum Science and Technology, 80799 München, Germany*

³*Department of Physics, Temple University, Philadelphia, Pennsylvania 19122, USA*

⁴*Fakultät für Physik, Ludwig-Maximilians-Universität, 80799 München, Germany*

(Dated: May 18, 2022)

We demonstrate a versatile, rotational-state dependent trapping scheme for the ground and first excited rotational states of $^{23}\text{Na}^{40}\text{K}$ molecules. Close to the rotational manifold of a narrow electronic transition, we determine tune-out frequencies where the polarizability of one state vanishes while the other remains finite, and a magic frequency where both states experience equal polarizability. The proximity of these frequencies of only 10 GHz allows for dynamic switching between different trap configurations in a single experiment, while still maintaining sufficiently low scattering rates.

Trapping potentials for ultracold atoms and molecules are based on spatially dependent energy shifts of their internal states produced by magnetic, electric, or optical fields. Generally, these energy shifts are state dependent, which greatly affects the time evolution of superposition states of atoms or molecules. Demand in precision quantum metrology, simulation and computation has motivated careful design of state-dependent traps that offer better control over quantum states. One limiting case is the magic trapping condition, where the light shift of two internal states is identical [1–3]. It is a key ingredient for achieving long coherence time in atomic and molecular clocks [4, 5]. Another limiting case is the tune-out condition, where the light shift of one state vanishes while the other remains finite [6, 7]. It can be used in novel cooling schemes for atoms [8], selective addressing and manipulation of quantum states [9–11], and precision measurements of atomic structure [12–17].

We extend these concepts to rotational states of ultracold polar molecules [18–27]. Such molecules offer unique possibilities for quantum engineering due to their strong long-range dipolar interactions and long single-particle lifetime [28–32]. Manipulating their rotational states is particularly important for experimental control of dipolar interactions. Though significant advances in controlling the internal states of molecules have been made [33–39], achieving long rotational coherence in optical dipole traps remains technically challenging as it requires careful control of trapping light polarization or intensity [40–42]. A magic-frequency trap can be used to reduce sensitivity to polarization angle or intensity fluctuation. Another major challenge for ultracold molecules are two-body loss processes originating from inelastic collisions that prevent effective evaporative cooling. For fermionic species, they can be suppressed by Pauli blocking in a three-dimensional lattice [43]. However, removing high entropy molecules from a lattice potential to achieve cooling in such a configuration is not straightforward. This problem could be solved with a tune-out lattice which traps

molecules in one state while letting others escape. In this work, we demonstrate a versatile rotational-state dependent trapping scheme that could be used to address such challenges by leveraging rotational transition lines of a nominally forbidden molecular transition.

In our experiments, we use $^{23}\text{Na}^{40}\text{K}$ molecules in their rovibrational ground state $|X^1\Sigma^+, v=0, J=0\rangle$ as well as their first rotationally excited state, $|J=1, m_J=0\rangle$. In the following, we will refer to these states as $|0\rangle$ and $|1\rangle$, respectively. The rotational-state dependent dipole trap is realized with laser light slightly detuned from the $|X^1\Sigma^+, v=0, J=0\rangle \leftrightarrow |b^3\Pi_0, v'=0, J'=1\rangle$ transition (subsequently called the $X \leftrightarrow b$ transition), which was previously studied in [44]. For detunings from this transition comparable to the rotational constants, dynamic polarizabilities depend strongly on the rotational level of the X state (see Fig. 1). Tune-out conditions for both states as well as a magic condition can thereby be achieved within a frequency range of less than 10 GHz. All intermediate ratios of polarizability can be realized between these limiting cases. The $X \leftrightarrow b$ transition is mostly electric-dipole forbidden and therefore exhibits a narrow partial linewidth of $\Gamma = 2\pi \times 297(10)$ Hz, much smaller than the spacing between rotational states. This leads to photon scattering rates small enough to realize dipole traps at the tune-out and magic frequencies.

The frequency of the $X \leftrightarrow b$ transition is $\omega_0 = 2\pi \times 346.123\,61(5)$ THz, corresponding to a wavelength of $\lambda = 866.1427(2)$ nm. The polarizabilities $\alpha_0(\Delta)$ and $\alpha_1(\Delta)$ of a molecule in $|0\rangle$ or $|1\rangle$, respectively, in a light field detuned by Δ from the $X \leftrightarrow b$ transition can be described by

$$\alpha_0 = -\frac{3\pi c^2}{2\omega_0^3} \frac{\Gamma}{\Delta} + \alpha_{\text{iso}}, \quad (1)$$

$$\alpha_1 = -\frac{3\pi c^2}{2\omega_0^3} \left(\frac{\Gamma \cos^2 \theta}{\Delta + 2(B+B')/\hbar} + \frac{1}{5} \frac{\Gamma(\cos^2 \theta + 3)}{\Delta - 2(2B' - B)/\hbar} \right) + \alpha_{\text{iso}} + \alpha_{\text{ang}}(\theta). \quad (2)$$

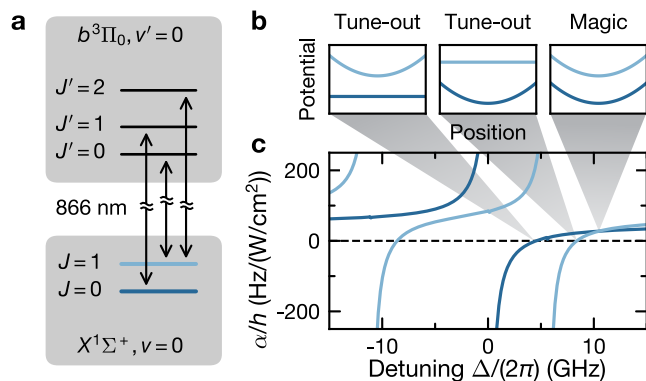


FIG. 1. Overview of the rotational-state dependent trapping scheme near the $X \leftrightarrow b$ transition. (a) Level diagram of the NaK molecule containing the $X \leftrightarrow b$ transition and the two nearest transitions from $|1\rangle$. (b) Schematic depiction of the potential experienced by $|0\rangle$ (dark blue) and $|1\rangle$ (bright blue) molecules in a dipole trap at the tune-out detuning for $|0\rangle$ (left panel), a tune-out detuning for $|1\rangle$ (center panel) and the magic detuning (right panel). (c) Frequency-dependent polarizability for $|0\rangle$ (dark blue) and $|1\rangle$ (bright blue), assuming light polarization parallel to the quantization axis. Each pole corresponds to one of the transitions shown in (a).

Here, α_{iso} and $\alpha_{\text{ang}}(\theta)$ are background terms that describe the polarization-independent and -dependent contributions from the other far-detuned transitions, respectively, and θ denotes the angle between the light polarization and the quantization axis, which is given by the direction of the dc electric field in the experiment. The background polarizability terms can be expressed as [2, 41, 45]

$$\alpha_{\text{iso}} = \frac{1}{3} \left(\alpha_{\text{bg}}^{\parallel} + 2\alpha_{\text{bg}}^{\perp} \right), \quad (3)$$

$$\alpha_{\text{ang}} = \frac{2}{15} (3 \cos^2 \theta - 1) (\alpha_{\text{bg}}^{\parallel} - \alpha_{\text{bg}}^{\perp}), \quad (4)$$

where $\alpha_{\text{bg}}^{\parallel}$ and $\alpha_{\text{bg}}^{\perp}$ are the background parallel and perpendicular polarizabilities, respectively. The photon scattering rate of molecules in $|0\rangle$ near the $X \leftrightarrow b$ transition is given by

$$\gamma_{\text{sc}} = \frac{3\pi c^2}{2\hbar\omega_0^3} \frac{\Gamma_e}{\Delta^2} I, \quad (5)$$

where I is the light intensity and Γ_e is the natural linewidth of the excited state, expected to be $\Gamma_e \approx 3\Gamma$ if the decay of the excited state to states other than the ground vibrational state is negligible as is the case for KRb molecules [46].

Our experimental cycle begins with the preparation of a near-degenerate sample of molecules in the $|0\rangle$ state using STIRAP as described in [47]. Depending on the measurement, this preparation is done either in a far-detuned crossed-beam optical dipole trap or a one- or three-dimensional (1D or 3D) optical lattice, described in

detail in the Supplemental Material [48]. The $1/e$ radius of the molecule cloud is $\approx 30 \mu\text{m}$. In order to image the molecules, we perform a reverse STIRAP procedure and employ absorption imaging on molecules in the resulting Feshbach molecule state [FB]. To measure the effect of light at small detuning from the $X \leftrightarrow b$ transition on the molecules, we illuminate them with a laser beam at a given detuning Δ . This beam is subsequently called the 866-nm beam and is provided by a Ti:Sapphire laser locked to a wavelength meter with a systematic error of less than 50 MHz [49]. This systematic error is considered in all frequency errors given in the following. The 866-nm beam is focused to a spot of $1/e^2$ radius $75 \mu\text{m}$, such that molecules experience an average intensity I of up to 2700 W/cm^2 .

To directly measure the frequency-dependent polarizability $\alpha_0(\Delta)$ of molecules in the state $|0\rangle$, we prepared molecules in the crossed dipole trap. The 866-nm beam was turned on during one of the STIRAP pulses and the resulting shift of the STIRAP two-photon resonance was used to determine α_0 as described in the Supplemental Material [48]. We found that α_0 agrees well with the theory curve as shown in Fig. 2(a).

In order to trap molecules in an optical dipole trap with long lifetime, the photon scattering rate must be low. We measured the radiative lifetime by illuminating molecules in state $|0\rangle$ with 866-nm light. The molecules were frozen in a far-detuned 3D optical lattice to avoid collisional loss. The molecule loss caused by the 866-nm beam was determined by fitting an exponential decay curve to the measured molecule numbers, see Fig. 2(b). From these data, we determined the position of the resonance feature at $\omega_0 = 2\pi \times 346.123\,61(5) \text{ THz}$. To ensure that this resonance was not shifted by the presence of far off-resonant dipole trap light, we performed additional loss measurements for small values of Δ with all far-detuned trapping light turned off and found a shift in resonance frequency of less than 20 MHz. Interestingly, we found the measured molecule loss rates to be an order of magnitude larger than the calculated photon-scattering rate according to Eq. (5). Two-photon processes were ruled out as a reason for the increased loss rate: On the one hand, the molecule loss rate γ_L scales linearly with I , excluding an excitation process with two 866-nm photons, see inset of Fig. 2(b). On the other hand, we did not observe a reduction of γ_L in absence of the far off-resonant trapping light, which rules out bichromatic two-photon processes. A possible explanation for the increased loss rate is that the decay of the b state to states other than $|X^1\Sigma^+, v=0\rangle$, e.g. to the $a^3\Sigma^+$ manifold, is dominant compared to the nominally forbidden $X \leftrightarrow b$ transition, leading to an increased natural linewidth Γ_e and therefore a larger photon scattering rate γ_{sc} . Unexpectedly, at $\Delta = 2\pi \times 1.83(5) \text{ GHz}$ we also observed a second, smaller loss peak which could not be attributed so far. Still, at all detunings relevant for rotational-state dependent

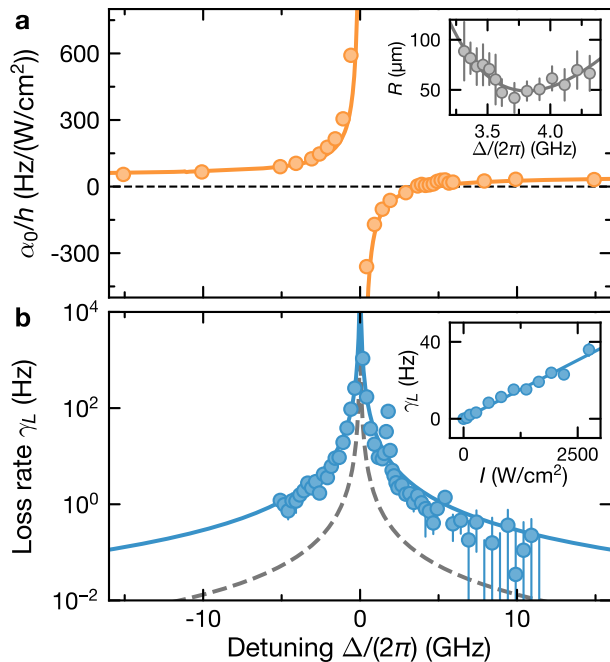


FIG. 2. Polarizability and loss rate of molecules in state $|0\rangle$. (a) Experimental data for polarizability $\alpha_0(\Delta)$ (orange circles) and theoretical curve determined using parameters from intensity-independent measurements (orange line.) The black dashed line indicates zero. Inset: Determination of the tune-out detuning for $|0\rangle$ by measuring cloud size after resonant heating. Grey circles are root-mean-square cloud sizes and the solid line is a fit used to find the minimum, see [48]. (b) Observed loss rate γ_L of molecules in $|0\rangle$ subjected to 866-nm light at an intensity of 1150 W/cm^2 (blue circles). The loss rate at $I = 0$ was subtracted from these data points. The blue solid line is a fit of Eq. 5 with Γ_e as the fit parameter, the grey dashed line shows the prediction of the photon scattering rate γ_{sc} assuming $\Gamma_e = 3\Gamma$. Error bars denote the standard error of the fit. Inset: Intensity dependence of the loss rate at $\Delta = 2\pi \times 1 \text{ GHz}$. The solid line is a linear fit to the data.

trapping, we find loss rates low enough that lifetimes of more than 1 s can be achieved in a 866-nm trap with a depth of $k_B \times 1 \mu\text{K}$.

To identify the tune-out detuning for the $|0\rangle$ state, we first prepared molecules in the crossed dipole trap. The 866-nm beam was additionally turned on and modulated for 160 ms with 100% peak-to-peak amplitude at a frequency of 110 Hz, equal to the strongest heating resonance of the dipole trap. After this procedure, we measured the molecule cloud size by determining the root-mean-squared deviation of the density distribution, R , after 0.6 ms time of flight. At $\alpha_0(\Delta) = 0$, the heating effect is minimized, so that the smallest cloud size should be observed. With the data shown in the inset of Fig. 2(a), the tune-out point was determined to be located at $\Delta_0^{(0)} = 2\pi \times 3.73(8) \text{ GHz}$.

To determine quantities associated with the excited

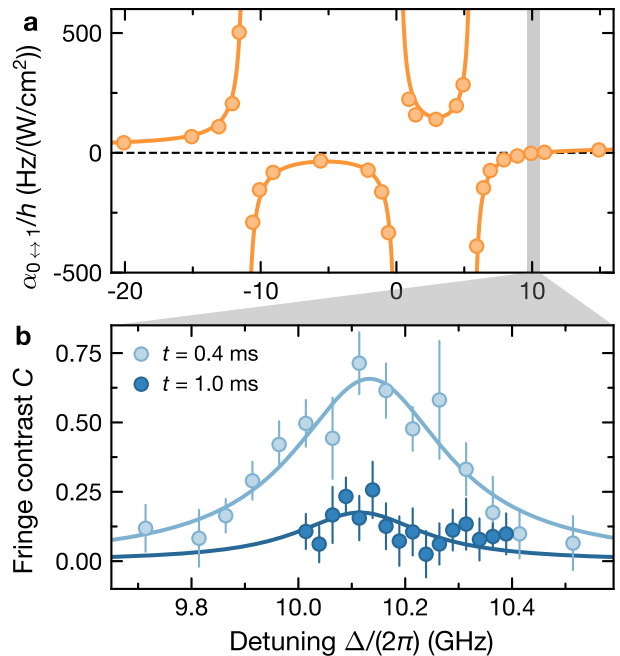


FIG. 3. Differential polarizability and magic detuning. (a) Experimental data for differential polarizability $\alpha_{0\leftrightarrow 1}$ from microwave spectroscopy (orange circles) and fit to the data (orange line). (b) Determination of the magic detuning via Ramsey spectroscopy. Bright (dark) blue circles are experimentally measured contrast after free evolution time $t = 0.4 \text{ ms}$ (1.0 ms) in the presence of 866-nm light. Lines are Lorentzian fits to the respective data sets, used to determine the center. Error bars denote one standard deviation and are determined from the covariance matrix of the fits.

rotational state $|1\rangle$, we trapped molecules in a spin-decoupled 1D magic lattice described in [41]. We employed a homogeneous electric field of 86 V/cm such that the angle between the polarization of the 866-nm light and the electric field was $4(2)^\circ$. The differential polarizability $\alpha_{0\leftrightarrow 1} = \alpha_1 - \alpha_0$ was measured via microwave spectroscopy as described in the Supplemental Material [48]. The resulting data agree with Eqns. (1) and (2), see Fig. 3(a).

The magic detuning can be accurately measured via Ramsey spectroscopy of the $|0\rangle \leftrightarrow |1\rangle$ transition, which consists of two resonant $\pi/2$ microwave pulses separated by a free evolution period with duration t . We varied the phase ϕ of the second microwave pulse for a given t to obtain Ramsey fringes. The population $N_0(\phi)$ of molecules that are projected back to the $|0\rangle$ state by the second microwave pulse changes periodically with ϕ . During the free evolution period, the 866-nm beam was turned on. Any inhomogeneous broadening of the microwave resonance due to the differential light shift of the 866-nm light reduces the contrast of N_0 . Therefore, the magic detuning is identified as the maximum of fringe contrast. By fitting a Lorentzian to the contrast data,

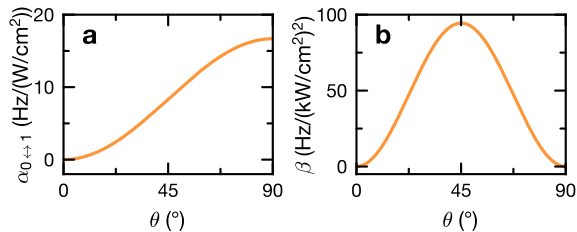


FIG. 4. Dependence of differential light shift on light polarization at the magic detuning with a dc electric field of 86 V/cm. (a) Theoretical differential polarizability $\alpha_{0\leftrightarrow 1}$ as a function of polarization angle θ . (b) Theoretical hyperpolarizability β of molecules in $|1\rangle$ as a function of polarization angle θ .

see Fig. 3(b), we determined the magic detuning to be $\Delta_m = 2\pi \times 10.11(6)$ GHz. In these measurements, the coherence time is limited to about 1 ms by residual inhomogeneities of the electric field. We expect a much longer coherence time by compensating the electric field gradient and trapping the molecules in a magic-frequency lattice. The benefit of our setup is that for 0- and 90-degree angles between the laser-field polarization and the quantization axis, the derivative of the polarizability with respect to the angle is zero, making our scheme robust against polarization imperfections. At the same time, this allows us to minimize differences in hyperpolarizability of rotational levels thereby further minimizing decoherence, see Fig. 4.

We can uniquely determine the shape of the polarizability curve $\alpha_0(\Delta)$ from two frequencies that were measured in an intensity-independent manner. The first of these is the tune-out detuning $\Delta_0^{(0)}$. The second is the point where the two-photon detuning of STIRAP between the Feshbach molecule state $|FB\rangle$ and the state $|0\rangle$ becomes insensitive to the 866-nm light intensity. This is achieved at a detuning Δ^* where molecules in $|FB\rangle$ and $|0\rangle$ experience the same light shift [48]. From these two measured detunings and the value of ω_0 , we computed the partial linewidth of the $X \leftrightarrow b$ transition Γ as well as the isotropic background polarizability α_{iso} via Eq. (1). The location of the poles of Eq. (2) and the known ground state rotational constant B were used to determine the excited state rotational constant B' . To find the values of the background polarizability terms $\alpha_{\text{bg}}^{\parallel}$ and $\alpha_{\text{bg}}^{\perp}$, we used the known form of $\alpha_0(\Delta)$ as well as Eqns. (3)-(4) and required the differential polarizability $\alpha_{0\leftrightarrow 1}$ to be zero at the measured value of Δ_m . Finally, using Γ and the background polarizability terms, we determined the two tune-out detunings of the state $|1\rangle$ to the left and the right of the $J = 1 \leftrightarrow J' = 2$ transition, $\Delta_0^{(1),l}$ and $\Delta_0^{(1),r}$. In combination, these quantities, summarized in Table I, fully describe the behaviour of molecules in the presence of light near the $X \leftrightarrow b$ transition.

Our results open new ways to address challenges in the

TABLE I. Summary of the molecular response at the $X \leftrightarrow b$ transition.

Quantity	Value	Reference
ω_0	$2\pi \times 346.123\,61(5)$ THz	This work
	$2\pi \times 346.1434$ THz	[44]
Γ	$2\pi \times 297(10)$ Hz	This work
$\alpha_{\text{bg}}^{\parallel}$	$h \times 106(6)$ Hz/(W/cm ²)	This work
$\alpha_{\text{bg}}^{\perp}$	$h \times 21(3)$ Hz/(W/cm ²)	This work
B'	$h \times 2.79(2)$ GHz	This work
	$h \times 2.85$ GHz	[44]
B	$h \times 2.821\,729\,7(10)$ GHz	[36]
$\Delta_0^{(0)}$	$2\pi \times 3.73(8)$ GHz	This work
$\Delta_0^{(1),l}$	$-2\pi \times 8.97(15)$ GHz	This work
$\Delta_0^{(1),r}$	$2\pi \times 7.91(15)$ GHz	This work
Δ_m	$2\pi \times 10.11(6)$ GHz	This work
Δ^*	$-2\pi \times 6.82(16)$ GHz	This work

field of ultracold polar molecules. For example, trapping molecules in a lattice at one of the tune-out wavelengths would allow selective transfer of hotter molecules at the edge of the lattice into the non-trapped state, thus removing entropy from the sample. In such a lattice, the molecules could thermalize via long-range interactions and would be protected from collisional loss by Pauli blocking [43] or dipole blocking [50]. Another natural application is to create repulsive potentials for ultracold molecules, e.g. to trap them in the dark. Due to the low photon scattering rates at small positive detuning from the $X \leftrightarrow b$ transition, one can generate a repulsive box trap with a potential barrier of $k_B \times 4\mu\text{K}$ at $\Delta = 2\pi \times 1$ GHz. The intensity in the trap's center can be as low as several W/cm², enough to allow investigation of the proposed photon-assisted loss of scattering complexes of molecules [51].

In conclusion, we demonstrated a versatile rotational-state dependent optical dipole trap by utilizing a nominally forbidden electronic transition from the singlet ground state to the lowest electronically excited triplet state of $^{23}\text{Na}^{40}\text{K}$ molecules. We precisely determined a tune-out frequency for the ground state molecules by resonant modulation heating spectroscopy and a magic frequency of rotational states by Ramsey interferometry. These frequencies are so close that dynamical switching between different trapping configurations is possible. The larger than expected photon scattering rate indicates that previously neglected decay channels may play an important role for the lifetime of the excited state. However, long lifetimes of ground-state molecules can still be achieved, e.g. at the magic frequency, the radiative molecule loss rate is as low as 0.1 Hz per $k_B \times \mu\text{K}$ trap depth. Our methods can be generalized to other species of ultracold bi-alkali molecules by carefully choosing a similar narrow molecular transition.

We thank Y. Bao, H. Bekker, A. Christianen, O.

Dulieu, J. He, T. Shi, D. Wang, and T. Zelevinsky for stimulating discussions. We thank C. Gohle, F. Seeßelberg, and S. Eustice for their contributions to the experiment. The MPQ team gratefully acknowledges support from the Max Planck Society, the European Union (PASQuanS Grant No. 817482) and the Deutsche Forschungsgemeinschaft under Germany's Excellence Strategy EXC-2111 390814868 and under Grant No. FOR 2247. Work at Temple University is supported by the Army Research Office Grant No. W911NF-17-1-0563, the U.S. Air Force Office of Scientific Research Grant No. FA9550-14-1-0321 and the NSF Grant No. PHY-1908634.

* roman.bause@mpq.mpg.de

- [1] H. Katori, T. Ido, and M. Kuwata-Gonokami, *J. Phys. Soc. Jpn.* **68**, 2479 (1999).
- [2] S. Kotochigova and D. DeMille, *Phys. Rev. A* **82**, 063421 (2010).
- [3] B. Neyenhuis, B. Yan, S. A. Moses, J. P. Covey, A. Chotia, A. Petrov, S. Kotochigova, J. Ye, and D. S. Jin, *Phys. Rev. Lett.* **109**, 230403 (2012).
- [4] J. Ye, H. J. Kimble, and H. Katori, *Science* **320**, 1734 (2008).
- [5] S. S. Kondov, C.-H. Lee, K. H. Leung, C. Liedl, I. Majewska, R. Moszynski, and T. Zelevinsky, *Nat. Phys.* **15**, 1118 (2019).
- [6] L. J. LeBlanc and J. H. Thywissen, *Phys. Rev. A* **75**, 053612 (2007).
- [7] B. Arora, M. S. Safronova, and C. W. Clark, *Phys. Rev. A* **84**, 043401 (2011).
- [8] J. Catani, G. Barontini, G. Lamporesi, F. Rabatti, G. Thalhammer, F. Minardi, S. Stringari, and M. Inguscio, *Phys. Rev. Lett.* **103**, 140401 (2009).
- [9] S. Kotochigova and E. Tiesinga, *Phys. Rev. A* **73**, 041405 (2006).
- [10] Y. Wang, X. Zhang, T. A. Corcovilos, A. Kumar, and D. S. Weiss, *Phys. Rev. Lett.* **115**, 043003 (2015).
- [11] A. Rubio-Abadal, J.-Y. Choi, J. Zeiher, S. Hollerith, J. Rui, I. Bloch, and C. Gross, *Phys. Rev. X* **9**, 041014 (2019).
- [12] W. F. Holmgren, R. Trubko, I. Hromada, and A. D. Cronin, *Phys. Rev. Lett.* **109**, 243004 (2012).
- [13] C. D. Herold, V. D. Vaidya, X. Li, S. L. Rolston, J. V. Porto, and M. S. Safronova, *Phys. Rev. Lett.* **109**, 243003 (2012).
- [14] A. Petrov, C. Makrides, and S. Kotochigova, *Mol. Phys.* **111**, 1731 (2013).
- [15] B. Henson, R. Khakimov, R. Dall, K. Baldwin, L.-Y. Tang, and A. Truscott, *Phys. Rev. Lett.* **115**, 043004 (2015).
- [16] W. Kao, Y. Tang, N. Q. Burdick, and B. L. Lev, *Opt. Express* **25**, 3411 (2017).
- [17] A. Heinz, A. J. Park, J. Trautmann, N. Šantić, S. G. Porsev, M. S. Safronova, I. Bloch, and S. Blatt, *arXiv:1912.10350*.
- [18] K.-K. Ni, S. Ospelkaus, M. H. G. de Miranda, A. Peer, B. Neyenhuis, J. J. Zirbel, S. Kotochigova, P. S. Julienne, D. S. Jin, and J. Ye, *Science* **322**, 231 (2008).
- [19] T. Takekoshi, L. Reichsöllner, A. Schindewolf, J. M. Hutson, C. R. L. Sauer, O. Dulieu, F. Ferlaino, R. Grimm, and H.-C. Nägerl, *Phys. Rev. Lett.* **113**, 205301 (2014).
- [20] P. K. Molony, P. D. Gregory, Z. Ji, B. Lu, M. P. Köppinger, C. R. L. Sauer, C. L. Blackley, J. M. Hutson, and S. L. Cornish, *Phys. Rev. Lett.* **113**, 255301 (2014).
- [21] J. W. Park, S. A. Will, and M. W. Zwierlein, *Phys. Rev. Lett.* **114**, 205302 (2015).
- [22] M. Guo, B. Zhu, B. Lu, X. Ye, F. Wang, R. Vexiau, N. Bouloufa-Maafa, G. Quémener, O. Dulieu, and D. Wang, *Phys. Rev. Lett.* **116**, 205303 (2016).
- [23] D. J. McCarron, M. H. Steinecker, Y. Zhu, and D. DeMille, *Phys. Rev. Lett.* **121**, 013202 (2018).
- [24] T. M. Rvachov, H. Son, A. T. Sommer, S. Ebadi, J. J. Park, M. W. Zwierlein, W. Ketterle, and A. O. Jamison, *Phys. Rev. Lett.* **119**, 143001 (2017).
- [25] H. Yang, D.-C. Zhang, L. Liu, Y.-X. Liu, J. Nan, B. Zhao, and J.-W. Pan, *Science* **363**, 261 (2019).
- [26] L. R. Liu, J. D. Hood, Y. Yu, J. T. Zhang, K. Wang, Y.-W. Lin, T. Rosenband, and K.-K. Ni, *Phys. Rev. X* **9**, 021039 (2019).
- [27] L. Anderegg, L. W. Cheuk, Y. Bao, S. Burchesky, W. Ketterle, K.-K. Ni, and J. M. Doyle, *Science* **365**, 1156 (2019).
- [28] L. D. Carr, D. DeMille, R. V. Krems, and J. Ye, *New J. Phys.* **11**, 055049 (2009).
- [29] M. A. Baranov, M. Dalmonte, G. Pupillo, and P. Zoller, *Chem. Rev.* **112**, 5012 (2012).
- [30] M. P. Kwasigroch and N. R. Cooper, *Phys. Rev. A* **96**, 053610 (2017).
- [31] J. L. Bohn, A. M. Rey, and J. Ye, *Science* **357**, 1002 (2017).
- [32] K.-K. Ni, T. Rosenband, and D. D. Grimes, *Chem. Sci.* **9**, 6830 (2018).
- [33] S. Ospelkaus, K.-K. Ni, G. Quémener, B. Neyenhuis, D. Wang, M. H. G. de Miranda, J. L. Bohn, J. Ye, and D. S. Jin, *Phys. Rev. Lett.* **104**, 030402 (2010).
- [34] B. Yan, S. A. Moses, B. Gadway, J. P. Covey, K. R. A. Hazzard, A. M. Rey, D. S. Jin, and J. Ye, *Nature* **501**, 521 (2013).
- [35] P. D. Gregory, J. Aldegunde, J. M. Hutson, and S. L. Cornish, *Phys. Rev. A* **94**, 041403 (2016).
- [36] S. A. Will, J. W. Park, Z. Z. Yan, H. Loh, and M. W. Zwierlein, *Phys. Rev. Lett.* **116**, 225306 (2016).
- [37] A. Prehn, M. Ibrügger, R. Glöckner, G. Rempe, and M. Zeppenfeld, *Phys. Rev. Lett.* **116**, 063005 (2016).
- [38] M. Guo, X. Ye, J. He, G. Quémener, and D. Wang, *Phys. Rev. A* **97**, 020501 (2018).
- [39] L. Caldwell, H. J. Williams, N. J. Fitch, J. Aldegunde, J. M. Hutson, B. E. Sauer, and M. R. Tarbutt, *arXiv:1908.11839*.
- [40] P. D. Gregory, J. A. Blackmore, J. Aldegunde, J. M. Hutson, and S. L. Cornish, *Phys. Rev. A* **96**, 021402 (2017).
- [41] F. Seeßelberg, X.-Y. Luo, M. Li, R. Bause, S. Kotochigova, I. Bloch, and C. Gohle, *Phys. Rev. Lett.* **121**, 253401 (2018).
- [42] J. A. Blackmore, L. Caldwell, P. D. Gregory, E. M. Bridge, R. Sawant, J. Aldegunde, J. Mur-Petit, D. Jaksch, J. M. Hutson, B. E. Sauer, M. R. Tarbutt, and S. L. Cornish, *Quantum Sci. Technol.* **4**, 014010 (2018).
- [43] A. Chotia, B. Neyenhuis, S. A. Moses, B. Yan, J. P. Covey, M. Foss-Feig, A. M. Rey, D. S. Jin, and J. Ye,

- Phys. Rev. Lett. **108**, 080405 (2012).
- [44] H. Harker, P. Crozet, A. J. Ross, K. Richter, J. Jones, C. Faust, J. Huennekens, A. V. Stolyarov, H. Salami, and T. Bergeman, Phys. Rev. A **92**, 012506 (2015).
- [45] M. Li, A. Petrov, C. Makrides, E. Tiesinga, and S. Kotochigova, Phys. Rev. A **95**, 063422 (2017).
- [46] J. Kobayashi, K. Aikawa, K. Oasa, and S. Inouye, Phys. Rev. A **89**, 021401 (2014).
- [47] F. Seeßelberg, N. Buchheim, Z.-K. Lu, T. Schneider, X.-Y. Luo, E. Tiemann, I. Bloch, and C. Gohle, Phys. Rev. A **97**, 013405 (2018).
- [48] See Supplemental Material for the theory of molecule polarizability, details on the experimental setup, fit functions for tune-out and magic frequencies, intensity calibration, example data for polarizability and lifetime measurements, and polarization dependence of polarizability, which includes Refs. [52–56].
- [49] L. Couturier, I. Nosske, F. Hu, C. Tan, C. Qiao, Y. H. Jiang, P. Chen, and M. Weidemüller, Rev. Sci. Instrum. **89**, 043103 (2018).
- [50] A. Micheli, G. Pupillo, H. P. Büchler, and P. Zoller, Physical Review A **76**, 043604 (2007).
- [51] A. Christianen, M. W. Zwierlein, G. C. Groenenboom, and T. Karman, Phys. Rev. Lett. **123**, 123402 (2019).
- [52] R. V. Krems, *Molecules in Electromagnetic Fields: From Ultracold Physics to Controlled Chemistry* (John Wiley & Sons, 2018).
- [53] M. E. Gehm, K. M. O'Hara, T. A. Savard, and J. E. Thomas, Phys. Rev. A **58**, 3914 (1998).
- [54] R. Vexiau, D. Borsalino, M. Lepers, A. Orbán, M. Aymar, O. Dulieu, and N. Bouloufa-Maafa, Int. Rev. Phys. Chem. **36**, 709 (2017).
- [55] R. Grimm, M. Weidemüller, and Y. B. Ovchinnikov, in *Advances In Atomic, Molecular, and Optical Physics* (Elsevier, 2000) pp. 95–170.
- [56] M. Safronova, B. Arora, and C. Clark, Phys. Rev. A **73**, 043401 (2006).

SUPPLEMENTAL MATERIAL

Theoretical description of polarizability and loss rate

The matrix elements of the effective molecular Hamiltonian for detuned laser-molecule interaction can be written as

$$\langle i | H_{\text{dip}} | i \rangle = \sum_j \frac{\hbar |\Omega_{ji}|^2}{4\Delta_{ji}}, \quad (\text{S1})$$

using second-order perturbation theory while neglecting the counter-rotating terms. Here, $\Omega_{ji} = \langle j | \hat{\mathbf{d}} \cdot \boldsymbol{\epsilon} | i \rangle E_0 / \hbar$ is the Rabi frequency of an electric field with amplitude E_0 and polarization $\boldsymbol{\epsilon}$ on a dipole-allowed transition between states $|i\rangle$ and $|j\rangle$, $\hat{\mathbf{d}} = \hat{d} \sum_q \sqrt{\frac{4\pi}{3}} Y_{1,q} \mathbf{e}^q$ is the dipole-moment operator with \hat{d} the corresponding one in the molecular frame, $Y_{l,m}$ are spherical harmonics, and \mathbf{e}^q are the spherical basis unit vectors where $q = 0, \pm 1$. The laser detuning Δ_{ji} is defined as $(E_j - E_i) / \hbar - \omega$ where E_j and E_i are the unperturbed energies of state $|j\rangle$ and $|i\rangle$ respectively, and ω is the laser photon frequency.

Now we suppose $|i\rangle$ is one of the two states of interest in the ground vibronic state. When $|i\rangle$ is effectively decoupled from any other energetically nearby states, as realized in the spin-decoupled setup [41], we can approximate its polarizability as

$$\alpha_i \approx \frac{-\langle i | H_{\text{dip}} | i \rangle}{I} = - \sum_j \frac{z_{ji}^2}{2\hbar\epsilon_0 c \Delta_{ji}}, \quad (\text{S2})$$

with the laser field intensity I and $z_{ji} = |\langle j | \hat{\mathbf{d}} \cdot \boldsymbol{\epsilon} | i \rangle|$.

In Born-Oppenheimer approximation, the wavefunction of $|i\rangle$ can be written as $|i\rangle = |X^1\Sigma^+\rangle |v=0\rangle |J, m_J\rangle$. We use the standard convention where a molecular state is described by $(^{2S+1})\Lambda_{\Omega}^{\pm}$ with the quantum numbers S as spin, Λ as the projection of orbital electronic angular momentum onto the molecular axis, and Ω as the projection of the total electronic angular momentum onto the molecular axis.

To study laser frequency dependence of polarizability near the narrow $X \leftrightarrow b$ transition, we focus on the contribution from the upper states of the $X \leftrightarrow b$ transition, which we call $|j'\rangle$, in the summation in Eq. (S2). The contribution from the rest of the states can be approximated to be constant with respect to laser frequency within tens of GHz of detuning from the central frequency ω_0 , and is encapsulated in background terms. The wavefunction of $|j'\rangle$ can be written similarly as $|j'\rangle = |b'\rangle |v'=0\rangle |J', m'_J\rangle$, where $|b'\rangle$ is the electronic wavefunction which mainly has $b^3\Pi_0$ character, but also has $A^1\Sigma^+$ character mixed in due to spin-orbit coupling. We can write it as $|b'\rangle = c_1 |b^3\Pi_0\rangle + c_2 |A^1\Sigma^+\rangle$. It is such mixing that gives the non-zero dipole matrix element between the ground states and $|j'\rangle$.

The q part of the matrix element of the dipole-moment operator between $|i\rangle$ and $|j'\rangle$ can be written as [52]

$$\begin{aligned} & \sqrt{\frac{4\pi}{3}} \mathbf{e}^q \langle b', v', J', m'_J | \hat{d} Y_{1,q} | X^1\Sigma^+, v, J, m_J \rangle = \\ & \sqrt{\frac{4\pi}{3}} \mathbf{e}^q c_2 \langle A^1\Sigma^+, v' | \hat{d} | X^1\Sigma^+, v \rangle \sum_p \sqrt{(2J+1)(2J'+1)} \\ & \times \begin{pmatrix} J' & 1 & J \\ -m'_J & q & m_J \end{pmatrix} \begin{pmatrix} J' & 1 & J \\ -\Lambda' & p & \Lambda \end{pmatrix}, \quad (\text{S3}) \end{aligned}$$

where $c_2 \langle A^1\Sigma^+, v' | \hat{d} | X^1\Sigma^+, v \rangle$ is the Franck-Condon overlap, p is the projection of the scattered photon's angular momentum onto the molecular axis, and S, Σ , and Λ are the angular momentum quantum numbers corresponding to the ground and excited electronic states. Since $\Lambda = \Lambda' = 0$ for $X^1\Sigma^+$ and $A^1\Sigma^+$, we have

$$\begin{aligned} & \langle b', v', J', m'_J | \hat{d} Y_{1,q} | X^1\Sigma^+, v, J, m_J \rangle = \\ & d_0 \sqrt{(2J'+1)(2J+1)} \\ & \times \begin{pmatrix} J' & 1 & J \\ -m'_J & q & m_J \end{pmatrix} \begin{pmatrix} J' & 1 & J \\ 0 & 0 & 0 \end{pmatrix}, \quad (\text{S4}) \end{aligned}$$

where $d_0 = c_2 \langle A^1\Sigma^+, v'=0 | \hat{d} | X^1\Sigma^+, v=0 \rangle$.

For state $|0\rangle$, the main contribution to the frequency-dependent part of the polarizability comes from $|b^3\Pi_0, v'=0, J'=1\rangle$, and contributions of all other excited states can be approximated with a constant α_{iso} , defined in the main text. From Eq. (S2) and (S4), we have

$$\alpha_0 = - \frac{2\pi d_0^2}{9\hbar\epsilon_0 c \Delta} + \alpha_{\text{iso}} = - \frac{3\pi c^2 \Gamma}{2\omega_0^3 \Delta} + \alpha_{\text{iso}}, \quad (\text{S5})$$

where we introduce the partial linewidth of the transition

$$\Gamma = \frac{\omega_0^3}{3\pi\epsilon_0 \hbar c^3} z_{ji}^2 = \frac{4\omega_0^3 d_0^2}{27\epsilon_0 \hbar c^3}. \quad (\text{S6})$$

For state $|1\rangle$, the frequency-dependent part of the polarizability comes from the states $|b^3\Pi_0, v'=0, J'=0, 2\rangle$, and the frequency-independent part is given by $\alpha_{\text{iso}} + \alpha_{\text{ang}}(\theta)$, as defined in the main text. Unlike for the $|0\rangle$ ground state, the polarizability of $|1\rangle$ depends on the light polarization. For linearly polarized light with polarization parallel to the quantization axis we have $\boldsymbol{\epsilon}_z = \mathbf{e}^0$, and for polarization perpendicular to the quantization axis we have $\boldsymbol{\epsilon}_x = (\mathbf{e}^1 + \mathbf{e}^{-1}) / \sqrt{2}$. With a polarization angle θ , the polarization unit vector can be written as $\boldsymbol{\epsilon} = \boldsymbol{\epsilon}_z \cos \theta + \boldsymbol{\epsilon}_x \sin \theta$. Along with Eq. (S2) and (S4), we arrive at the equation for α_1 in the main text.

The photon scattering rate of state $|i\rangle$ is given by

$$\gamma_i = \sum_j \frac{\Omega_{ji}^2}{4\Delta_{ji}^2} \Gamma_j, \quad (\text{S7})$$

where Γ_j is the natural linewidth of $|j\rangle$. For state $|0\rangle$,

$$\gamma_{sc} = \frac{3\pi c^2 \Gamma \Gamma_e}{2\hbar\omega_0^3 \Delta^2} I + c^{\text{bg}} I, \quad (\text{S8})$$

where Γ_e is the natural linewidth of $|b^3\Pi_0, v' = 0, J' = 1\rangle$, and $c^{b^3}I$ includes the contribution from all other excited states which can be neglected when the laser is near-detuned. We can write Γ_e as a sum of partial linewidths of different decay channels. The decay to different rotational states $|i\rangle$ of $|X^1\Sigma^+, v = 0\rangle$ is given by

$$\Gamma_{e,v=0} = \sum_i \frac{1}{3\pi\epsilon_0\hbar c^2} z_{ji}^2 = \frac{4\omega_0^3 d_0^2}{9\epsilon_0\hbar c^3} = 3\Gamma. \quad (\text{S9})$$

If other decay channels are neglected, we have $\Gamma_e \approx 3\Gamma$. The differential light shift between the $|0\rangle$ and $|1\rangle$ states can be approximated by [41]

$$\delta\omega_{0\leftrightarrow 1} = \frac{1}{\hbar}(\alpha_{0\leftrightarrow 1}(\theta)I + \beta(E, \theta)I^2 + \mathcal{O}(I^3)), \quad (\text{S10})$$

where θ is the polarization angle, $\alpha_{0\leftrightarrow 1}$ is the differential polarizability as defined in the main text, β is the hyperpolarizability of $|1\rangle$, and E is the magnitude of the applied dc electric field. An approximation for β can be derived by considering the contribution from four-photon couplings to the $|X^1\Sigma^+, v = 0, J = 1, m_J = \pm 1\rangle$ states and back. It reads

$$\beta(\theta, E) = \frac{5B}{3d^2E^2}(\alpha_1(0) - \alpha_1(\pi/2))^2 \sin^2(2\theta), \quad (\text{S11})$$

where $d = 2.72 \text{ D}$ is the permanent dipole moment of $^{23}\text{Na}^{40}\text{K}$.

Experimental setup

Molecule association is performed after preparing a mixture of $\sim 10^5$ ^{23}Na and ^{40}K atoms each, at a temperature of 300 nK and a magnetic field of 85.4 G in the vertical (z) direction. We then apply a radiofrequency pulse to create molecules in a weakly bound Feshbach molecule state $|\text{FB}\rangle$ and use STIRAP as described in [47] to create molecules in the rovibrational ground state $|0\rangle$. This association procedure can be done either in a far-detuned crossed-beam optical dipole trap or in a 1D or 3D optical lattice. The crossed dipole trap consists of a 1064-nm and a 1550-nm laser beam intersecting orthogonally in the horizontal (x - y) plane. The trap frequencies experienced by molecules in $|0\rangle$ in this trap are (94, 72, 233) Hz in the (x, y, z)-directions, respectively. The 1D lattice is formed by a retro-reflected 1550-nm laser beam and is magic for the $|0\rangle \leftrightarrow |1\rangle$ transition. As described in [41], this is achieved by applying a dc electric field in the y -direction, which serves to decouple the rotational states, the hyperfine states, and the trapping light field, and by aligning the polarization of the lattice light with a magic angle relative to this electric field. The 3D lattice is used to suppress collisional loss in experiments that require long molecule lifetimes. It is formed by three retro-reflected laser beams: In the vertical direction, the

wavelength is 1550 nm and the beam size is $100 \mu\text{m}$, allowing for lattice depths of up to $800 E_R$ for ground state molecules, where E_R is the photon-recoil energy for these molecules in a lattice of the respective wavelength. In both horizontal directions, the wavelength is 1064 nm and the beam size is $300 \mu\text{m}$. The maximal lattice depth in these directions is $200 E_R$. The 866-nm beam is focused onto the molecules along the z -direction. Except in the measurements to determine the polarization dependence of the differential polarizability, the polarization of this beam is always at an angle of $4(2)^\circ$ to the y -direction, almost parallel to the dc electric field.

Tune-out detuning determination

As described in the main text, the tune-out detuning $\Delta_0^{(0)}$ for molecules in state $|0\rangle$ was identified as the detuning where the minimum of heating occurs when modulating the 866-nm beam at the heating resonance of the crossed dipole trap. The heating process depends on the sample temperature as well as the modulation amplitude and modulation frequency. When the temperature of molecules is much smaller than the trap depth and the modulation is weak, the heating can be described as an exponential increase in the sample's energy with a time constant $\Gamma_h = S\alpha_0^2(\Delta)I_{\text{mod}}^2$ [53], where S depends on the modulation frequency and I_{mod} is the modulation amplitude of the intensity. For the case of strong heating, the temperature quickly saturates to an equilibrium where the heating is balanced by hot molecules escaping from the trap. However, for $\alpha_0(\Delta) \approx 0$, the exponential model can still be used. In linearized form, the expression for the cloud size R after modulating the 866-nm beam power at a given modulation frequency for a fixed time reads

$$R(\Delta) = R_0 + \xi \left(\frac{1}{\Delta} - \frac{1}{\Delta_0^{(0)}} \right)^2. \quad (\text{S12})$$

Here, R_0 is the initial cloud size and ξ is a constant which contains the dependence on intensity, modulation time and modulation frequency. We used this expression with R_0 , ξ , and $\Delta_0^{(0)}$ as fit parameters to determine the detuning at which the minimum of heating occurs and thereby find the tune-out detuning, as shown in the inset of Fig. 2(a) of the main text.

Magic condition between Feshbach and ground-state molecules

We also identified the magic detuning Δ^* from ω_0 where molecules in the Feshbach-molecule state $|\text{FB}\rangle$ and the rovibrational ground state $|0\rangle$ experience the same light shift in a way that is independent of the intensity

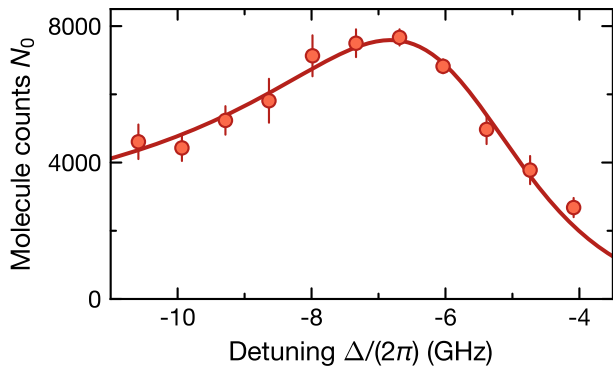


FIG. S1. Magic condition for $|FB\rangle$ and $|0\rangle$. Molecule number measured at zero STIRAP two-photon detuning and in the presence of 866-nm light at various Δ during STIRAP (red circles). The solid line is a fit of Eq. (S13). Error bars denote the standard error of the mean of 6 data points.

of the 866-nm light. To do this, 866-nm light at various values of Δ was turned on during one of the STIRAP pulses at a two-photon detuning which was calibrated to be resonant in the case with no 866-nm light. The individual light shifts of $|FB\rangle$ and $|0\rangle$ detune the STIRAP two-photon resonance and thereby lower the molecule-conversion efficiency unless $\alpha_0(\Delta)$ matches the polarizability α_{FB} of the molecules in $|FB\rangle$ at Δ^* . Because $|FB\rangle$ is a very weakly bound state, its polarizability can be computed to be $\alpha_{FB} = h \times 76.26 \text{ Hz}/(\text{W}/\text{cm}^2)$ by summing the polarizabilities of the constituent atoms [54–56]. This number is approximately independent of Δ because the molecular resonance is far below the lowest atomic resonances of ^{23}Na and ^{40}K . To determine Δ^* from the data, we model the drop in STIRAP conversion efficiency due to the shift of the STIRAP two-photon resonance as

$$N_0 = N_{\max} \frac{\Gamma_s^2/4}{\Gamma_s^2/4 + (I(\alpha_0(\Delta) - \alpha_{FB})/\hbar)^2}, \quad (\text{S13})$$

where N_0 is the number of molecules that we detect in state $|0\rangle$, N_{\max} is the number of detected molecules when the STIRAP two-photon transition is on resonance, and Γ_s is the linewidth of the STIRAP two-photon resonance. To obtain a fit function, the general form $\alpha_0(\Delta) = A/\Delta + \alpha_c$ was inserted into Eq. (S13), and N_{\max} , Γ_s , A , and α_c were used as fit parameters. We found the maximum conversion efficiency at $\Delta^* = -2\pi \times 6.82(16) \text{ GHz}$, see Fig. S1.

Intensity calibration

The intensity of the 866-nm light was calibrated from the measured light shift and the known polarizabilities of ground state molecules α_0 and of Feshbach molecules

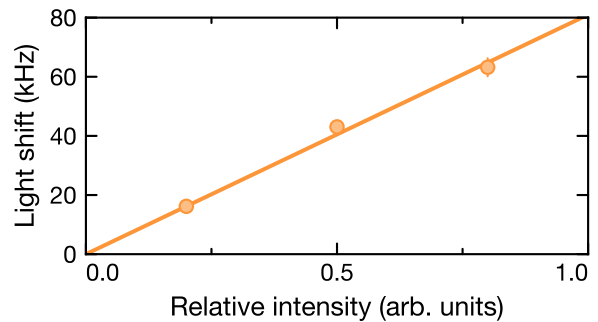


FIG. S2. Intensity calibration of the 866-nm light from known polarizability at $\Delta = 2\pi \times 80 \text{ GHz}$. Differential light shift between $|0\rangle$ and $|FB\rangle$ measured via STIRAP two-photon resonance shift $\delta\omega_{FB\leftrightarrow 0}$ for different intensities. Circles denote the center frequencies of Lorentzian fits to the spectra recorded at each intensity, error bars are derived from the covariance matrix of the fit. The line is a linear fit to the center frequencies.

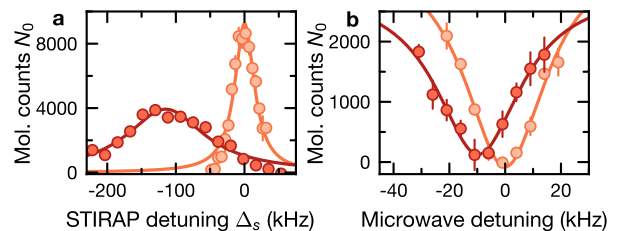


FIG. S3. Example data for polarizability measurements. (a) Determination of α_0 via STIRAP two-photon resonance shift. The 866-nm beam was turned on during STIRAP. Data were taken at $\Delta = -2\pi \times 2 \text{ GHz}$ and $I = 1200 \text{ W}/\text{cm}^2$ (dark red) and compared to a calibration measurement with the 866-nm light turned off (bright red). (b) Determination of differential polarizability $\alpha_{0\leftrightarrow 1}$ via microwave spectroscopy. Data were taken at $\Delta = 2\pi \times 3 \text{ GHz}$ and $I = 69 \text{ W}/\text{cm}^2$ (dark red) and compared to a calibration measurement taken with the 866-nm light turned off (bright red). The solid lines are Lorentzian fits. Error bars denote the standard error of the mean of 3 to 4 data points.

α_{FB} at $\Delta = 2\pi \times 80 \text{ GHz}$ according to

$$\hbar\delta\omega_{FB\leftrightarrow 0} = (\alpha_0(2\pi \times 80 \text{ GHz}) - \alpha_{FB})I \quad (\text{S14})$$

as shown in Fig. S2. Specifically, we used the value $\alpha_0(2\pi \times 80 \text{ GHz}) = h \times 47(1) \text{ Hz}/(\text{W}/\text{cm}^2)$, which was obtained from the previous measurements of $\Delta_0^{(0)}$ and Δ^* . We found $2700(100) \text{ W}/\text{cm}^2$ at 100% relative power.

Polarizability measurements

The polarizability $\alpha_0(\Delta)$ of molecules in state $|0\rangle$ was determined from the observed shift of STIRAP two-photon resonance Δ_s that occurred when turning the

866-nm beam on during one of the STIRAP pulses. Example data is shown in Fig. S3(a). The shift of two-photon detuning is equal to the differential light shift $\hbar\delta\omega_{\text{FB}\leftrightarrow 0}(I, \Delta)$ between the |FB) and |0) states. From this, we obtained $\alpha_0(\Delta)$ via

$$\alpha_0(\Delta) = \alpha_{\text{FB}} - \hbar\delta\omega_{\text{FB}\leftrightarrow 0}(I, \Delta)/I. \quad (\text{S15})$$

The precision of this method is limited by drifts of the STIRAP two-photon resonance, which we compensated as far as possible by performing regular calibration measurements without 866-nm light.

The differential polarizability $\alpha_{0\leftrightarrow 1}$ was measured via microwave spectroscopy. After the association of molecules in the state |0) in the magic 1D lattice, their rotational state can be changed to |1) via a resonant microwave π -pulse with a duration of 35 μs . This can be observed as molecule loss because molecules in |1) are not resonant with the reverse STIRAP. The light shift $\hbar\delta\omega_{0\leftrightarrow 1}(\Delta)$ of the |0) \leftrightarrow |1) transition caused by the presence of 866-nm light during the microwave pulse then yields $\alpha_{0\leftrightarrow 1}(\Delta)$ by

$$\alpha_{0\leftrightarrow 1}(\Delta) \equiv \alpha_1(\Delta) - \alpha_0(\Delta) = \hbar\delta\omega_{0\leftrightarrow 1}(\Delta)/I. \quad (\text{S16})$$

Example data for a scan of the microwave transition frequency is shown in Fig. S3(b). For all polarizability measurements, the intensity of the 866-nm light was chosen in order to achieve a compromise between the magnitude of the light shift and the inhomogeneous broadening caused by the finite size of the 866-nm beam. For the measurements of α_0 , the intensities we used were between 360 W/cm^2 and 2200 W/cm^2 . The measurements of $\alpha_{0\leftrightarrow 1}$ were performed at intensities between 70 W/cm^2 and 550 W/cm^2 .

Polarization dependence

The polarization dependence of the polarizability $\alpha_{\text{ang}}(\theta)$ was determined by measurements of the differential polarizability $\alpha_{0\leftrightarrow 1}$ at a constant detuning $\Delta = 2\pi \times 80$ GHz and at various angles between the laser polarization and the electric field, see Fig. S4. At this detuning, $\alpha_{0\leftrightarrow 1} = \alpha_{\text{ang}}(\theta)$ is a good approximation. The results agree well with the prediction of Eq. (5) in the main text as well with the values determined for $\alpha_{\text{bg}}^{\parallel}$ and $\alpha_{\text{bg}}^{\perp}$ in Table I of the main text.

Lifetime measurements

Data on molecule lifetime in the presence of 866-nm light was obtained by holding molecules in the |0) state in a deep 3D lattice. The association was done at lattice depths of 150 E_R in the vertical direction and 15 - 20 E_R

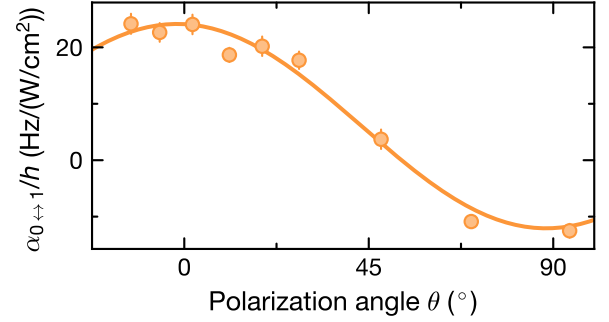


FIG. S4. Dependence of differential polarizability $\alpha_{0\leftrightarrow 1}$ on the angle θ between laser polarization and electric field. The measurements were performed at a detuning $\Delta = 2\pi \times 80$ GHz. Error bars denote the standard error of the mean of 4 to 8 data points. The solid line is a fit of Eq. (4) in the main text.

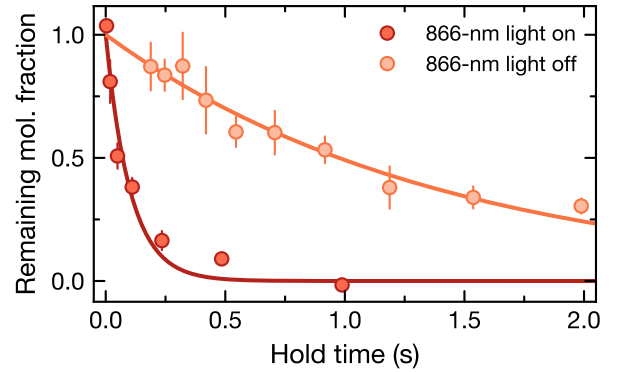


FIG. S5. Example data for lifetime measurements in a 3D lattice in the presence of 866-nm light at a detuning $\Delta = -2\pi \times 1.5$ GHz and intensity $I = 1150$ W/cm^2 are shown in dark red. The measurement of the background loss rate in the deep 3D lattice is shown in bright red. Circles are experimental data, error bars denote the standard error of the mean of 3 to 4 data points, and the solid lines are exponential fits to determine the $1/e$ lifetime.

in the horizontal direction. After molecule association, the lattice was ramped to 40 (120) E_R in the vertical (horizontal) direction over 100 ms for the data points at detunings $\Delta \geq 2\pi \times 1$ GHz. This is the lattice configuration in which we observed the longest $1/e$ lifetime of ground-state molecules of 1.4 s. For data points at detunings $\Delta < 2\pi \times 1$ GHz, no additional lattice ramp was performed, resulting in a molecule lifetime of 0.17 s. The 866-nm beam was then ramped on over a time of 50 μs to an intensity of 1150 W/cm^2 and the molecules were held for various durations before imaging, see Fig. S5. For each data point presented in Fig. 2(b) of the main text, the loss rate measured in the respective lattice configuration in absence of 866-nm light was subtracted.

Ramsey spectroscopy

Ramsey spectroscopy was used to determine the magic frequency, at which the smallest dephasing occurs for superpositions of the states $|0\rangle$ and $|1\rangle$. 866-nm light at a given detuning was turned on during the free evolution time t . To mitigate a damped and chirped interference fringe due to the fast drift of the electric field and molecule loss, instead of changing t between measurements, we varied the phase ϕ of the second microwave pulse for a given t . The fringe contrast C and initial phase ϕ_0 were determined by fitting the function

$$N_0(\phi) = \frac{N_{\text{tot}}(t)}{2} (1 - C(t) \cos(\phi + \phi_0)) \quad (\text{S17})$$

to the measured molecule numbers, see example data shown in Fig. S6.

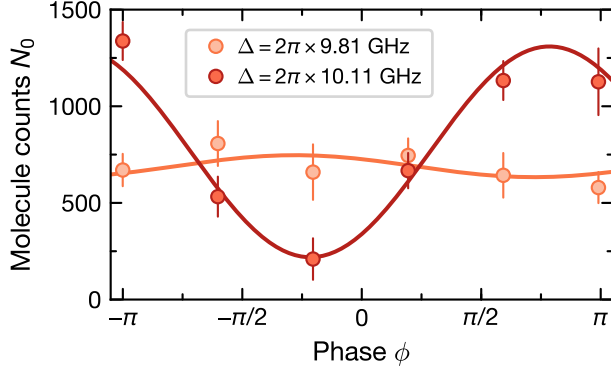


FIG. S6. Example data for determination of the magic detuning via Ramsey spectroscopy. Data were taken after 0.4 ms free evolution time at detunings $\Delta = 2\pi \times 9.81$ GHz (bright circles) and $\Delta = 2\pi \times 10.11$ GHz (dark circles). Error bars denote the standard error of the mean of 4 data points. The solid lines are fits of Eq. (S17).